Atmos. Chem. Phys. Discuss., doi:10.5194/acp-2016-44, 2016
Manuscript under review for journal Atmos. Chem. Phys.
Published: 9 March 2016

Atmospheric Chemistry and Physics Discussions

Modeling the Diurnal Variability of Agricultural Ammonia in Bakersfield, California during CalNex

C. R. Lonsdale[1], J. D. Hegarty[1], K. Cady-Pereira[1], M. J. Alvarado[1], D. K. Henze[2], M. D. Turner[2], S. L. Capps[2], J. B. Nowak[3,4,*], J. A. Neuman[4], A. M. Middlebrook[4], R. Bahreini[4], J. G. Murphy[5], M. Markovic[5,3], T. C. VandenBoer[5**], L. M. Russell[6], A. J. Scarino[7]

[1]Atmospheric and Environmental Research, Lexington, MA, USA
[2]Department of Mechanical Engineering, University of Colorado, Boulder, CO, USA
[3]Cooperative Institute for Research in Environmental Sciences, University of Colorado Boulder, CO, USA
[4]Chemical Sciences Division, Earth System Research Lab, NOAA, Boulder, CO, USA
[5]Department of Chemistry, University of Toronto, Toronto, ON Canada
[6]Scripps Institution of Oceanography, University of California, San Diego, CA, USA
[7]Science Systems and Applications Inc., Hampton, Virginia, USA
*Now at Aerodyne Research, Inc. Billerica, MA, USA
**Now at Air Quality Research Division, Environment Canada, Toronto, ON, CA

Correspondence to: C. R. Lonsdale (clonsdal@aer.com)

Abstract. NH_3 retrievals from the NASA Tropospheric Emission Spectrometer (TES), as well as surface and aircraft observations of $NH_{3(g)}$ and submicron $NH_{4(p)}$, are used to evaluate modelled concentrations of $NH_{3(g)}$ and $NH_{4(p)}$ from the Community Multiscale Air Quality (CMAQ) model in the San Joaquin Valley (SJV) during the California Research at the Nexus of Air Quality and Climate Change (CalNex) campaign. We find that simulations of NH_3 driven with the California Air Resources Board (CARB) CalNex emission inventory are qualitatively and spatially consistent with TES satellite observations, with a correlation coefficient (r^2) of 0.54. However, the surface observations at Bakersfield indicate a missing diurnal cycle in the model bias, with CMAQ overestimating surface NH_3 at night and underestimating it during the day. The surface, satellite, and aircraft observations all suggest that the afternoon NH_3 emissions in the CARB inventory are underestimated by at least a factor of two, while the night-time overestimate of $NH_{3(g)}$ is likely due to a combination of overestimated NH_3 emissions, underestimated deposition, and insufficient vertical mixing in the Weather Research and Forecasting model (WRF) meteorological fields used to drive CMAQ.

We used the surface observations at Bakersfield to derive an empirical diurnal cycle of NH_3 emissions in the SJV, in which night-time and midday emissions differed by about a factor of 4.5. Adding this diurnal profile to the CMAQ simulations while keeping the daily total NH_3 emissions constant at the CARB values significantly improved the model performance at night, but sizable errors (up to 15 ppbv) in night-time NH_3 remain, likely due to remaining errors in vertical mixing at night. The model performance is slightly degraded during the afternoon when the diurnal cycle is adjusted, but this may reflect relatively small (~20 %) errors in the total NH_3 emissions rather than remaining errors in the diurnal cycle. Running

Atmos. Chem. Phys. Discuss., doi:10.5194/acp-2016-44, 2016
Manuscript under review for journal Atmos. Chem. Phys.
Published: 9 March 2016

Atmospheric Chemistry and Physics Discussions

CMAQv5.0.2 with bi-directional NH_3 flux also improves model performance on a similar scale, while combining bi-directional NH_3 fluxes and adjusted emissions significantly reduces the model bias at night.

1 Introduction

The emissions of ammonia (NH_3) to the atmosphere are highly uncertain (e.g., Pinder et al., 2006; Beusen et al., 2008; Galloway et al., 2008; Henze et al., 2009; Schlesinger, 2009). Nitrogen dioxide (NO_x = NO + NO_2) and sulfur dioxide (SO_2) photoxidize in the atmosphere to form nitric acid (HNO_3) and sulfuric acid (H_2SO_4), respectively, which react with atmospheric gas-phase ammonia ($NH_{3(g)}$) to form ammonium sulfate ($(NH_4)_2SO_4$) and ammonium nitrate (NH_4NO_3) aerosol. Uncertainty in NH_3 emissions therefore leads to significant uncertainties in the concentrations of secondary inorganic aerosols. Ammonium sulfate and nitrate aerosols contribute to fine particulate matter concentrations ($PM_{2.5}$), and thus to decreased visibility, altered climate, and acidification and eutrophication in sensitive ecosystems (e.g., Paulot et al., 2014; RoTAP. 2012; Bricker et al., 2007; Martin et al., 2004).

$PM_{2.5}$ also causes adverse health effects (WHO, 2013; Pope et al., 2004). In particular, some regions in the San Joaquin Valley (SJV) in California have been designated as non-attainment areas for $PM_{2.5}$, with NH_3 emissions contributing to more than half of the inorganic $PM_{2.5}$ in the state (Schiferl et al., 2014), depending on ambient conditions and concentrations (Lonsdale et al., 2012). During the summer CalNex campaign, however, concentrations of $PM_{2.5}$ rarely exceeded the National Ambient Air Quality Standard (NAAQS) in the SJV, as $PM_{2.5}$ exceedances in the SJV generally happen in the winter. While emissions of NO_x and SO_2 are relatively well constrained, are regulated by the United States Environmental Protection Agency (US EPA), and are predicted to continually decrease due to air quality regulations and emission reducing technologies (US EPA, 2010), NH_3 emissions are not currently regulated and are predicted to stay constant or increase over the next several decades in the US due to an increasing population and the associated increase in farming and agricultural activities (Moss et al., 2010). Climate change is also predicted to increase NH_3 emissions (+ 0-40 % in north-central Europe) with larger countries having the largest uncertainty in emissions variations (Skjøth et al., 2013).

Anthropogenic NH_3 sources in the SJV are dominated by agricultural activities, with livestock waste estimated to contribute about 74 % of total anthropogenic NH_3 to the atmosphere and chemical fertilizer use another 16 % (Simon et al., 2008). Agricultural emissions of NH_3 can be highly variable due to factors such as the differences in fertilizer application, the diet provided to livestock, and the waste management and storage practices of farmers (Hristov et al., 2011; Sawycky et al., 2014). In addition, while $NH_{3(g)}$ can be quickly deposited to the surface causing soil acidification, water eutrophication, and an imbalance of ecosystems when in excess (e.g., Carfrae et al., 2004), the air-surface exchange of NH_3 is bidirectional, with the direction of the NH_3 flux between the land and the atmosphere varying with temperature, relative humidity, vegetation type, maintenance (e.g., cutting and tilling practices), and fertilizer applications (Nemitz et al., 2001; Zhang et al., 2010; Ellis et al., 2011; Bash et al., 2013; Sawycky et al., 2014). This complexity in the emission and deposition of NH_3, along with the rapid reactions of NH_3 with HNO_3 and H_2SO_4 and the consequently short (~1 day) atmospheric lifetime of NH_3 leads to large

Atmos. Chem. Phys. Discuss., doi:10.5194/acp-2016-44, 2016
Manuscript under review for journal Atmos. Chem. Phys.
Published: 9 March 2016

Atmospheric Chemistry and Physics Discussions

temporal and spatial variability of this gas, as seen in in situ measurements (e.g., Langford et al., 1992; Carmichael et al., 2003; Nowak et al., 2010; Walker et al., 2013) and in satellite retrievals (e.g., Clarisse et al., 2009; Pinder et al., 2011; Shephard et al., 2011; Heald et al., 2012; Sun et al., 2015; Shephard and Cady-Pereira, 2015).

Recent studies have recognized a diurnal pattern of NH_3 emissions from livestock attributed to potential differences in farm management practices, livestock housing outflow patterns, and variations in soil moisture, temperature and wind speed (Hensen et al., 2009; Zhu et al., 2015a; Zhu et al., 2015b). To account for this, a diurnal variability scheme was implemented into global simulations using the global 3-dimensional chemical transport model, GEOS-Chem, and was shown to decrease NH_3 concentrations globally (Zhu et al., 2015a). That study also calculated the bi-directional exchange of ammonia, which decreased NH_3 concentrations in the US in the months of October through April and increased it in the month of July (Zhu et al., 2015a). Bash et al. (2013) also explored the sensitivity of modelled NH_3 concentrations to a bi-directional ammonia scheme that used meteorological factors, including temperature, wind speed, agricultural crop flux values, and a nitrogen soil geochemistry parameterization in the CMAQ model. They found that over the continental US their model run with the bi-directional ammonia scheme decreased the total dry deposition of NH_3 by 45 %, thus increasing atmospheric NH_3 concentrations and NH_x wet deposition by 10 % and 14 %, respectively. Wichink Kruit et al. (2012) use the DEPosition of Acidifying Compounds (DEPAC) surface-atmospheric exchange module in a CTM and saw an increase in atmospheric NH_3 almost everywhere in their model domain, including decreased NH_3 deposition with a remaining underestimation in agricultural areas.

Previous studies have also shown that errors in NH_3 emissions are a common contributing factor to modelled $PM_{2.5}$ and NH_3 bias (e.g., Schiferl et al., 2014). Skjøth et al., (2011) discuss their method for calculating dynamic NH_3 emissions that include distributions of agricultural ammonia in Europe. Their method is designed for use in chemical transport models and their results show considerable improvements made in the agricultural ammonia sector, particularly areas with detailed records of agricultural practices. Inverse modelling studies have been used to reduce the uncertainty in NH_3 emissions as well, generally by assimilating surface observations of the wet deposition of ammonium (NH_4^+) in precipitation. Gilliland et al. (2003) used the CMAQ model to determine that the 1990 version of the US EPA National Emissions Inventory (NEI), which is based on emission estimates and model inputs from State, Local and Tribal agencies (US EPA, 2015), overestimated total emissions of NH_3 by 20 %. Gilliland et al. (2006) performed a similar study for the 2001 NEI and found that this updated inventory represented the total emissions of NH_3 well, but that NH_3 emissions needed to be increased in summer and reduced in winter. Henze et al. (2009) used the adjoint of the global chemical transport model GEOS-Chem to assimilate IMPROVE observations and found that the high nitrate concentrations in the model implied that total US NH_3 emissions for 1998 were overestimated.

More recently, satellite observations of NH_3 have been incorporated into inverse studies. By assimilating satellite retrievals of NH_3 concentrations from TES (Beer et al., 2008; Shephard et al., 2011) aboard the NASA Aura satellite, it has been found that NH_3 emission sources in GEOS-Chem are broadly underestimated (Zhu et al., 2013). Heald et al. (2012) and Walker et al. (2012) used the Inter Agency Monitoring of Protected Visual Environments (IMPROVE) network data and satellite

Atmos. Chem. Phys. Discuss., doi:10.5194/acp-2016-44, 2016
Manuscript under review for journal Atmos. Chem. Phys.
Published: 9 March 2016

Atmospheric Chemistry and Physics Discussions

retrievals of NH_3 from the Infrared Atmospheric Sounding Instrument (IASI, Van Damme et al., 2014) aboard the EUMETSAT MetOp-A satellite to show that NH_3 emissions are likely underestimated in GEOS-Chem for California, leading to a local underestimate of ammonium ($NH_{4(p)}$) aerosol. Other infrared nadir sounders have also been used to provide satellite observations of NH_3. For example, Shephard and Cady-Pereira (2015) demonstrated the ability of the Crosstrack Infrared Sounder (CrIS) aboard the joint NOAA-NASA Suomi National Polar-orbiting satellite to measure daily, spatially distributed tropospheric NH_3 in California, and in preliminary results found it correlated well with Deriving Information on Surface Conditions from Column and Vertically Resolved Observations Relevant to Air Quality (DISCOVER-AQ) measurements in the SJV in January 2013.

Investigating the formation, transport, and fate of $NH_{3(g)}$ and $NH_{4(p)}$ in California was one of the major goals of the NOAA CalNex field campaign performed in May and June 2010, which provided measurements from flights and surface sites. Nowak et al. (2012) used this data to demonstrate the importance of ammonium nitrate formation downwind of the Los Angeles urban core and dairy facilities further east. They found that NH_3 emissions from these dairy farms were underestimated by a factor of 3 or more, thus indicating the need for better representation in this emission sector. Kelly et al. (2014) in general saw well-correlated comparisons of CMAQ model estimates to measurements from the EPA's Chemical Speciation Network. Their model tended to under-predict NH_x ($NH_x = NH_{3(g)} + NH_{4(p)}$) during the day at the Bakersfield, CA site and significantly over-predict $NH_{3(g)}$ at night. They suggest that this model bias may be due to emissions from livestock and dairy farms being too low and lacking in variability in this region or to errors in crustal cation predictions and the missing effects of organic acids and amines on inorganic aerosol thermodynamics (Kelly et al., 2014).

Model estimates of the planetary boundary layer (PBL) height are essential in correctly quantifying atmospheric pollutant concentrations, especially for short-lived pollutants like NH_3. Such estimates are difficult at fine spatial and temporal scales, especially in the complex terrain of the SJV. Scarino et al. (2014) studied the PBL and mixed layer heights during CalNex using WRF and high spectral resolution lidar (HSRL) data taken during the campaign. They found that, in general, there is good agreement between the WRF modelled output and measured values; however, in the Central Valley there is a WRF mixed-layer height over-prediction and an inability to represent the diurnal growth of the mixed layer in the early part of the day. Additionally they suggest that future improvements will require a focus on mixing layer characteristics and soil moisture and temperature. Baker et al. (2013) explored how well the WRF model configuration used to drive the CMAQ simulations of Kelly et al. (2014) simulates PBL height during CalNex, using two versions of WRF. The study shows that both WRF versions simulate the PBL and mixing layers well within the SJV, as well as other large scale flow patterns, but under-predict local wind speed and temperature. A strong aerosol gradient is used to identify the top of the PBL in HSRL measurements, which may also be present in a night-time residual layer. Baker et al. (2013) take this into account by identifying the surface-attached mixed layer, which they assume as the lowest significant gradient in such a circumstance.

In this study, we use the CalNex observations of $NH_{3(g)}$ and aerosol ammonium ($NH_{4(p)}$) and the CMAQ model to evaluate the estimates of NH_3 emissions in the SJV contained in the California Air Resources Board (CARB) inventory (Figure 1a). While previous NH_3 model evaluation efforts using CalNex data have focused on the NEI inventory (Kelly et al., 2014;

Atmos. Chem. Phys. Discuss., doi:10.5194/acp-2016-44, 2016
Manuscript under review for journal Atmos. Chem. Phys.
Published: 9 March 2016

Atmospheric Chemistry and Physics Discussions

Heald et al., 2012; Walker et al., 2012), the CARB inventory is used in the development of California's State Implementation Plans (SIPs) under the Clean Air Act, and so ensuring the accuracy of this emission inventory is important to the design of air quality policy for the SJV and California in general. In addition, previous studies have not taken advantage of the high-resolution observations of $NH_{3(g)}$ made by the TES satellite instrument over Bakersfield during the CalNex campaign. Here we evaluate the consistency of the satellite, aircraft, and surface observations of $NH_{3(g)}$ and $NH_{4(p)}$ during the CalNex campaign and then use these observations, along with lidar retrievals of PBL height, to investigate the biases in the magnitude and diurnal cycle of emissions of $NH_{3(g)}$ and $NH_{4(p)}$ from the CARB inventory in the SJV. We also explore the sensitivity of modelled ammonia concentrations to bi-directional ammonia exchange using the bi-directional NH_3 flux scheme in CMAQv5.0.2.

Section 2 briefly describes the data sources used in this study, while Section 3 describes the CARB emission inventory and the configurations used for the WRF, HYSPLIT and CMAQ model runs in this study. The performance of the CARB inventory used in our CMAQ simulations, along with model sensitivity studies, is presented in Section 4. Section 5 discusses our suggested improvements to the CARB NH_3 inventory and summarizes our conclusions.

2 Data

2.1 NOAA CalNex campaign

The NOAA WP-3 aircraft completed 18 research flights during the CalNex campaign, which included measurements of $NH_{3(g)}$ and $NH_{4(p)}$. $NH_{3(g)}$ was measured at 1 s (~100 m) intervals using chemical ionization mass spectrometry (CIMS) with an uncertainty of +/- 30 % as described in detail in Nowak et al. (2010). Submicron $NH_{4(p)}$ was measured at 10 s (~ 1 km) intervals with an uncertainty of ~ 30 % using a compact time-of-flight aerosol mass spectrometer from Aerodyne (c-TOF AMS, Bahreini et al., 2009). In this study we focused on the flights of 7 and 24 of May and 16 and 18 of June when the WP-3 was sampling air in the SJV (Figure 1a). The quality-controlled flight data were reported at a merged time resolution of 1 s, which we averaged to 1 minute values (the approximate time it takes the WP-3 to cross a 4 km CMAQ grid box) and then matched the sample times and locations to the corresponding time and location of the CMAQ hourly concentration output.

2.1.1 Bakersfield surface observations

Bakersfield, California is located on the southern part of the SJV and there is a general north-to-south orographic air-flow in this region, with a tendency for emissions to get trapped in the valley due to the nearby mountains (seen in Figure 1a) (Baker et al., 2014). At the Bakersfield site the Ambient Ion Monitor Ion Chromatograph (AIM-IC, Ellis et al., 2010, Markovic et al., 2012) was used to measure $NH_{3(g)}$ at a frequency of 1 Hz and an uncertainty of +/- 20 %. In addition, size-resolved, sub-micron non-refractory $NH_{4(p)}$ measurements were taken at 5 minute intervals using an Aerodyne Aerosol Mass Spectrometer (AMS) (Ryerson et al., 2013). We averaged these data to 1 h time resolution in order to compare to the hourly CMAQ model output, which allowed for the evaluation of the ability of CMAQ to simulate the diurnal cycle of NH_3 concentrations. When

Atmos. Chem. Phys. Discuss., doi:10.5194/acp-2016-44, 2016
Manuscript under review for journal Atmos. Chem. Phys.
Published: 9 March 2016

Atmospheric Chemistry and Physics Discussions

particulate ammonium ($NH_{4(p)}$) measurements are available we compare model results to NH_x to reduce our sensitivity to gas-to-particle partitioning errors in the model, otherwise we compare to $NH_{3(g)}$.

2.2 TES NH_3 retrievals

During CalNex, TES made special observations (transects) near the Bakersfield, CA surface site with a horizontal separation of 12 km on six different afternoons. TES is a nadir-viewing Fourier-transform infrared (FTIR) spectrometer with a high spectral resolution of 0.06 cm^{-1} and a nadir footprint of 5.3 km x 8.3 km. TES flies aboard the NASA Aura spacecraft, which is in a sun-synchronous orbit with an equator crossing time around 01:30 and 13:30 local solar time. Beer et al. (2008) reported the first satellite observations of boundary layer $NH_{3(g)}$ using the TES instrument. Shephard et al. (2011) developed and tested a full $NH_{3(g)}$ retrieval algorithm. The retrieval is based on an optimal estimation approach that minimizes the differences between the TES Level 1B spectra and a radiative transfer calculation that uses absorption coefficients calculated with the AER line-by-line radiative transfer model LBLRTM (Clough et al., 2006). The a priori profiles and covariance matrices for TES NH_3 retrievals are derived from GEOS-Chem model simulations of the 2005 global distribution of NH_3.

The TES $NH_{3(g)}$ retrievals generally have a region of maximum sensitivity between 700 hPa and the surface. While the retrieval is performed on 14 pressure levels, the number of degrees of freedom for signal (DOFS) is generally not greater than one. Therefore at any given single profile level the retrieved volume-mixing ratio (VMR) of NH_3 is highly influenced by the a priori profile. Rather than attempting to analyse data from individual retrieval levels, it is often desirable to express the retrieved information in a representation where the influence of the a priori is reduced and the information available is collapsed to a single point. To address this issue, Shephard et al. (2011) developed a Representative Volume Mixing Ratio (RVMR) metric for $NH_{3(g)}$ based on similar techniques used previously for CH_4 (e.g., Payne et al., 2009; Wecht et al., 2012; Alvarado et al., 2015) and CH_3OH (e.g., Beer et al., 2008). This RVMR represents a TES sensitivity weighted average value where the influence of the a priori profile is reduced as much as possible; it generally ranges from 20 % to 60 % of the retrieved surface value for $NH_{3(g)}$. The minimum detection level for TES $NH_{3(g)}$ retrievals is an RVMR of approximately 0.4 ppbv, corresponding to a profile with a surface-mixing ratio of about 1-2 ppbv (Shephard et al., 2011).

Pinder et al. (2011) showed that the TES NH_3 retrievals were able to capture the spatial and seasonal variability of NH_3 over eastern North Carolina and that the retrievals compared well with in situ surface observations of NH_3, while Alvarado et al. (2011) showed that TES NH_3 retrievals can also capture the higher concentrations of NH_3 in forest fires in Canada. Sun et al. (2015) demonstrated that under optimal conditions (i.e., good thermal contrast and NH_3 amounts significantly above the TES level of detectability), TES NH_3 agreed very well with in situ aircraft and surface measurements taken in the California Central Valley during the Deriving Information on Surface Conditions from COlumn and VERtically Resolved Observations Relevant to Air Quality (DISCOVER-AQ) 2013 campaign.

There are at least three issues that have to be considered when using NH_3 satellite profiles to evaluate model predictions: (a) the vertical resolution of the satellite profile is substantially coarser than that of the model profile; (b) the DOFS for NH_3 are

Atmos. Chem. Phys. Discuss., doi:10.5194/acp-2016-44, 2016
Manuscript under review for journal Atmos. Chem. Phys.
Published: 9 March 2016

Atmospheric Chemistry and Physics Discussions

generally less than 1.0; and (c) the retrieved satellite profile reflects the influence of the choice of a priori profile (Rodgers and Connor, 2003). Thus, in order to use these TES observations to evaluate CMAQ model predictions of the concentrations of $NH_{3(g)}$, we first interpolate the hourly CMAQ NH_3 profile predicted for 13:00 local solar time (expressed as the natural logarithm of the mixing ratio) to the TES pressure grid. We then apply the TES observation operator to the interpolated CMAQ NH_3 profile to derive a model TES profile ($\boldsymbol{x}_{TES}$). Finally, we apply the sensitivity weighting to calculate the model RVMR ($CMAQ_{RVMR}$). This value represents the RVMR that would have been retrieved if (a) TES had sampled a profile identical to the CMAQ-simulated profile and (b) the retrieval errors due to jointly retrieved parameters, other model parameters, and instrument noise were negligible. The observation operator equation is

$$\boldsymbol{x_{TES}} = x_a + \mathbf{A}(\boldsymbol{x_{CMAQ}} - \boldsymbol{x_a}) \quad (1)$$

$$CMAQ_{RVMR} = \mathbf{W} * \boldsymbol{x_{TES}} \quad (2)$$

where $\boldsymbol{x_a}$ is a vector of the TES a priori NH_3 concentrations, $\mathbf{A}$ is the averaging kernel matrix, $\boldsymbol{x_{CMAQ}}$ is a vector of the interpolated CMAQ NH_3 values, and $\mathbf{W}$ is a weighting matrix (Rodgers and Connor, 2003; Payne et al., 2009).

2.3 PBL heights

Several studies have used lidar observations of aerosol profiles to determine the height of the planetary boundary layer (PBL) by identifying regions of large gradients in aerosol concentrations with height (e.g., Tucker et al., 2009; Lewis et al., 2013; Scarino et al., 2014; Hegarty et al., 2015). Scarino et al. (2014) and Tucker et al. (2009) define the mixed layer measured by the HSRL as 'the volume of atmosphere in which aerosol chemical species emitted within the boundary layer are mixed and dispersed'. The NASA Langley Research Center (LaRC) airborne HSRL measured mixed layer heights during May and June 2010 for the CalNex campaign and the Carbonaceous Aerosol and Radiative Effects Study (Scarino et al., 2014), both of which we used in this study.

3 Models

3.1 WRF-ARW

CMAQ v5.0.2 was driven with meteorology provided by WRF ARW Version 3.5 (Skamarock and Klemp, 2008) that was configured with 3 nested domains of 36, 12, and 4 km horizontal grid spacing and 41 vertical layers. Shortwave and longwave radiation were calculated using the RRTMG radiative transfer code (Mlawer et al., 1997; Iacono et al., 2008). The YonSie University (YSU, Hong et al., 2006) non-local turbulent PBL scheme and the Noah land surface scheme (Chen and Dudhia, 2001) were used. Initial and boundary conditions for WRF were provided by the North American Regional Reanalysis (NARR, Mesinger et al., 2006), which is recognized as state-of-the-science for North America (Bukovsky and Karoly, 2007). The WRF runs were 32-hour simulations initialized every 24 hours at 0000 UTC with analysis nudging of winds, temperature and humidity above the PBL on the inner 10 km domain as well as winds in the PBL as in Nehrkorn et

Atmos. Chem. Phys. Discuss., doi:10.5194/acp-2016-44, 2016
Manuscript under review for journal Atmos. Chem. Phys.
Published: 9 March 2016

Atmospheric Chemistry and Physics Discussions

al. (2013). The WRF outputs for UTC hours 09:00 to 32:00 from each consecutive simulation were combined to form a continuous time series and the initial 8 hours of each simulation were discarded as spin-up time. The 8-h spin-up time and 32-h simulation length is longer than the 6-h spin-up time and 30-h simulation length used by Nehrkorn et al. (2013), but were necessary to perform 24-hour daily CMAQ runs using the 24-h daily CARB emissions files that started at 8:00 UTC. The WRF output was then converted to CMAQ-model-ready files using the Meteorology-Chemistry Interface Processor version 4.2 (MCIP).

3.2 CMAQ

We ran CMAQ on the inner 4 km WRF domain using the SAPRC07 chemical mechanism (Hutzell et al., 2012, Carter et al., 2010ab), which corresponds to the model-ready emission files for CalNex provided by CARB, and with the CMAQ AERO6 aerosol module with aqueous chemistry. Biogenic emissions, photolysis rates, and deposition velocities were all calculated inline. There were few clouds in California during this study period and thus lightning NO_X emissions were negligible; however, lightning NO_x emissions were also calculated inline in CMAQ. Initial and horizontal boundary conditions for CMAQ were provided by GEOS-Chem simulations on a 2° x 2.5° latitude-longitude grid for May and June 2010 following the approach of Lapina et al. (2014).

CMAQ emissions inputs for the state of California were provided as model-ready files by CARB, which prepared them using the Modeling Emissions Data System on a 4 km x 4 km grid-scale (available at http://orthus.arb.ca.gov/calnex/data/calnex2010.html, last accessed January, 2016). The emission change log is provided at ftp://orthus.arb.ca.gov/pub/outgoing/CalNex/2010/modelready/Change Log for Posted Inventories.pdf (last accessed January, 2016). In this inventory, the NH_3 emissions in SJV are assumed to be constant throughout the day (i.e., no diurnal cycle), and are constant day-to-day in a given month. NH_3 emissions in the SoCAB did have a strong diurnal cycle, as about 75 % of the NH_3 emissions were coded as "industrial" and only emitted between 8 AM and 4 PM local time. As these emissions were mainly due to sewage treatment, this diurnal cycle assumption is likely incorrect. However, evenly distributing these SoCAB emissions across the day had little impact on NH_3 in the SJV. As the CARB model-ready files had no out-of-state emission sources, our initial simulations were run using the CARB emissions for California, the GEOS-Chem boundary conditions, and no out-of-state emissions. We quantified the potential error in gas-phase $NH_{3(g)}$, Aitken and Accumulation mode aerosol $NH_{4(p)}$, and NH_x in the SJV from neglecting out-of-state agricultural NH_3 emissions by using the agricultural NH_3 emissions from the NEI2011 platform, which we re-gridded from 12 km to our model's 4 km scale while keeping California state emissions constant. We performed this sensitivity test for a 7-day case study between 25-31 May with a 4-day spin up in order to correspond to in situ measurements and two of the TES transects. Adding these out-of-state emissions had a negligible impact on the modelled NH_3 concentrations in the SJV (less than 0.001 % change), as the prevailing winds are mostly out of the north and northwest. Additionally, we tested the effect that errors in the boundary conditions from GEOS-Chem might have on the model runs. Doubling NH_3 boundary conditions for the same 10-day case

Atmos. Chem. Phys. Discuss., doi:10.5194/acp-2016-44, 2016
Manuscript under review for journal Atmos. Chem. Phys.
Published: 9 March 2016

Atmospheric Chemistry and Physics Discussions

study also had little impact on NH_3 concentrations in the SJV (less than 0.001 % change), which was expected based on the short lifetime of NH_3.

Finally, we also ran CMAQv5.0.2 using the bi-directional exchange scheme for ammonia developed by Bash et al. (2013) with results discussed in Section 4.4. This tool uses the U. S. Department of Agriculture's Environmental Policy and Integrated Climate (EPIC) model (Bash et al., 2013), which uses fertilizer application data, crop type, soil type, and meteorology from MCIP output to calculate soil emissions potential and NH_4.

3.3 HYSPLIT

In order to explore the sources influencing the Bakersfield concentrations we ran the Hybrid Single-Particle Lagrangian Integrated Trajectory (HYSPLIT) model. Using meteorological inputs from the WRF 4 km domain discussed in Section 3.1, we generated 36-hour back trajectories with Version 4 of the HYSPLIT model (Draxler and Hess, 1998) initiated from 100 m above ground level (agl) at Bakersfield at 17:00 PDT on June 18th back to 20:00 PDT on June 17th. Results from these runs are discussed in Section 4.3.

4 Results

4.1 Evaluation of modelled boundary layer $NH_{3(g)}$ with TES NH_3 retrievals

Figure 2a shows the RVMR retrieved from the TES spectra (TES_{RVMR}) for one overpass on 12 May 2010. Figure 2b shows the equivalent modelled NH_3 RVMR ($CMAQ_{RVMR}$) (see Equation 1 and 2 in Section 2.2), and Figure 2c shows the difference between the two. We can see that CMAQ with the CARB emission inventory does a good job of representing the locations of different sources of NH_3 and the resulting relative changes in NH_3 along the transect, but that the NH_3 RVMRs are underestimated, particularly at higher NH_3 RVMRs. Figure 3 is a scatterplot of the modelled and measured RVMR for all six transects near Bakersfield, with the footprints closest to Bakersfield marked in green. The modelled and measured RVMRs are reasonably well correlated (r^2 of 0.54 and mean bias of -2.68 ppbv), again suggesting that CMAQ with the CARB inventory does a good job of capturing the spatial distribution of NH_3 emissions near Bakersfield. However the slope of the linear regression of modelled to measured NH_3 RVMR suggests that CMAQ underestimates high NH_3 concentrations by a factor of 2.4.

4.2 Evaluation of modelled NHx diurnal cycle and vertical distribution

Figure 4a shows the average hourly ratio of modelled versus measured NH_x concentrations for the Bakersfield ground site, averaged over all days of the CalNex campaign, which is derived from the boxplots shown in Figure 4b. We are plotting NH_x here so as to include the effects of gas-to-particle partitioning, discussed later in this section. The CMAQ model runs with the CARB emission inventory generally underestimate NH_x during the daytime by about a factor of 2.5, consistent with the average TES RVMR observations near Bakersfield at about 13:30 local solar time plotted as the green dot in Figure 4a.

Atmos. Chem. Phys. Discuss., doi:10.5194/acp-2016-44, 2016
Manuscript under review for journal Atmos. Chem. Phys.
Published: 9 March 2016

Atmospheric Chemistry and Physics Discussions

However, this model underestimate is not constant throughout the day. Instead it shows a clear diurnal cycle, with CMAQ significantly overestimating surface NH_x concentrations at night by up to a factor of 4.5. The overall magnitude of measured concentrations generally increases from May to June (not shown), possibly due to increasing temperatures. This suggests that the constant daily emissions for agricultural NH_3 emissions in the CARB inventory may be misrepresenting the diurnal emission patterns seen in the measurements, which is consistent with previous work done in North Carolina: Wu et al. (2008) also found that NH_3 emissions from livestock feed lots show a strong diurnal cycle, peaking at mid-day. This also demonstrates the importance of using highly time-resolved observations of NH_3 to determine the diurnal cycle of NH_3 before using polar-orbiting satellite retrievals of NH_3 to improve the spatial and seasonal distribution of the emissions, as noted in Zhu et al. (2013). In other words, if we had relied on the TES observations at 13:30 local solar time to evaluate the CMAQ runs with the constant CARB diurnal profile of NH_3 emissions, we would have incorrectly assumed that the CARB inventory was a factor of 2.4 too low for total NH_3 emissions, whereas the surface data demonstrate that the problem is primarily in the diurnal cycle of the emissions.

Besides errors in emissions another contributing factor to misrepresentation of modelled $NH_{3(g)}$ could be errors in the gas-to-particle partitioning of $NH_{3(g)}$ to $NH_{4(p)}$. Figure 4a also shows an average hourly plot of the ratio of measured to modelled NH_x, along with $NH_{3(g)}$ during the campaign. There is very little difference between the two lines, indicating only a small fraction of the total $NH_{3(g)}$ is being converted into $NH_{4(p)}$ in this region, consistent with Baker et al. (2013). Thus, errors in gas-particle partitioning of NH_3 in CMAQ, while important for accurately estimating $PM_{2.5}$ concentrations, cannot account for the diurnal errors in NH_x we have observed.

The aircraft observations in the SJV also indicate a large underestimate (range of 1.4 to 7.1) in NH_x concentrations, as shown in Table 1 (all flights in SJV) and Figure 5 (two flights). The variation in model concentrations in the background of the plot are due to the aircraft flying in and out of horizontal and vertical grid boxes. The May 24th flight shows a strong CMAQ NH_x underestimate of about a factor of 5 when considering the entire flight with an r^2 value of 0.4 and mean bias of -1.95 ppbv. This significant underestimate could partly be due to the underestimate of vertical mixing at night (discussed below); when only data before 18:00 PDT is considered (assuming this is before the collapse of the convective boundary layer) the underestimate is only a factor of ~1.5 and the r^2 is 0.77, a considerably better result. However, model comparisons to flight data on 16 and 18 of June before 18:00 PDT, likely before the boundary layer collapse on these days, show a significant model underestimate and low r^2 values; thus there may be other contributing factors to this bias. When looking at $NH_{3(g)}$ and $NH_{4(p)}$ separately, $NH_{4(p)}$ has a large absolute mean bias for all flights, but its low magnitude has a negligible effect on NH_x concentrations (see Table 1).

Early afternoon (Figure 5a) and evening (Figure 5b) model runs and flight measurements show a clear difference in vertical distribution of NH_x. At night (May 24th flight), the model contains most of the NH_x in the lowest model grid, whereas during the day (June 16th flight) it vertically mixes NH_x. The aircraft measurements suggest 1) vertical mixing is happening during both flights, based on the higher NH_x concentrations that the aircraft is measuring at higher altitudes, 2) or that there is a residual layer of NH_x at night that is not captured by the model or 3) there is a non-local source that is also not well captured

Atmos. Chem. Phys. Discuss., doi:10.5194/acp-2016-44, 2016
Manuscript under review for journal Atmos. Chem. Phys.
Published: 9 March 2016

by the model. Model comparison to flight measurements are constrained by mismatch errors caused by the difference in temporal and spatial resolutions, since the model output is only every hour on a horizontal grid spacing of 4 km.

Another potential source of diurnal errors in NH_x concentrations are diurnal variations in meteorology, which could potentially alter the source regions to which the Bakersfield site was sensitive throughout the day. Differences in NH_3 emission errors at upwind sites would thus appear as diurnal errors in NH_x. Figure 6 shows a case study for June 18th, where HYSPLIT back trajectories were run for eight different times during the day (only 4 shown). As on most days during the CalNex campaign, there is a general flow from the north/north-west during the day and night that is funnelled through the California Central Valley towards Bakersfield. In these simulations, as well as in other runs on different days (not shown), there is no significant change in meteorology with time of day, and thus diurnal changes in transport are not likely a contributing factor to the diurnal mismatch shown in modelling results. Back trajectories for other days (not shown) all support this assessment and also indicate a consistent general flow from the north/north-west passing through the PBL of the California Central Valley in the previous 24 hours. The back trajectories arriving at Bakersfield on the 18 of June indicate that the air would have been funnelled into the valley through the gap in the coastal range adjacent to San Francisco Bay, with lighter winds occurring at night-time. These back trajectories, driven with our WRF model data, did not show a change in source attribution locations and are in general agreement with those generated with the NAM12 and EDA40 operational analyses (not shown).

Finally, diurnal errors in the PBL height estimates could potentially be responsible for the diurnal pattern in the CMAQ NH_x concentrations at Bakersfield discussed above. We used daytime HSRL measurements taken in the SJV during CalNex to evaluate our WRF simulated PBL heights. Figure 7 shows the WRF PBL plotted against the HSRL calculated mixed layer, which contains PBL heights both manually chosen based on the aerosol profile and using the Brooks algorithm (Scarino et al., 2014). Results for the three daytime flights that passed over the SJV had a slope of 0.91, r^2 of 0.45 and mean bias of 45 m, and thus errors in daytime ML height cannot account for the underestimate in modelled daytime NH_x. Scarino et al. (2014), when comparing all CalNex HSRL flight measurements to their configuration of the WRF-Chem model, obtained a similar result with a slope of 0.58 and r^2 of 0.3; however, this result was for all flights, not just those in the SJV region.

In summary, gas-to-particle partitioning and PBL height errors are likely not responsible for the diurnally-varying measurement to model biases. The daytime high bias is most likely due to an underestimation of daytime emissions. However, the aircraft observations of NH_x in the SJV suggest that the vertical mixing in CMAQ at night is too low to reasonably simulate night-time surface concentrations of NH_x. This suggests that the observed CMAQ overestimate of NH_x at night is due to a combination of an overestimate of the night-time emissions, an underestimate of night-time deposition and an underestimate in vertical mixing at night.

4.3 Sensitivity to diurnal variability in emissions

The solid blue line in Figure 8a shows that the CARB NH_3 emissions in the SJV are mostly constant, both diurnally and day-to-day, with an hourly flux of around 0.23 moles s^{-1} for the Bakersfield 16 km^2 grid box. The Bakersfield ground

Atmos. Chem. Phys. Discuss., doi:10.5194/acp-2016-44, 2016
Manuscript under review for journal Atmos. Chem. Phys.
Published: 9 March 2016

Atmospheric Chemistry and Physics Discussions

measurements, however, indicate there should be a diurnal pattern of lower emissions at night and higher emissions during the day, as has been previously reported of NH_3 emissions from livestock (e.g., Bash et al., 2013; Zhu et al., 2015) and based on more detailed information regarding agricultural ammonia sectors (Skjøth et al., 2011) which the current CARB emissions inventory does not have. In order to test this hypothesis, we applied a scaling factor to all NH_3 area sources per grid box in the SJV, based on the CMAQ bias relative to the ground observations at Bakersfield (see Figure 4) and consistent with measured temperature patterns. To do this, we first calculated the total NH_3 area source emissions for each grid box, based on additional information on the emissions breakdown from the CARB inventory. We then calculated the emissions for each hour based on the hourly average ground measurements. Note that the adjusted maximum emissions vary by about a factor of 5 from the minimum at night to the mid-day peak, as can be seen in Figure 8a (solid red line) which is more modest than the factor of 10 variation seen in feedlots (Bash et al., 2013; J. Bash, personal communication, Oct. 6, 2015). We then reran CMAQ for a 7-day period during the CalNex campaign (May 25-31, with a previous 4-day spin-up) to assess the impact that this diurnal cycle had on the model bias. The overall diurnal cycle of this 7-day period was similar to the full campaign average, with a peak around mid-day; however the maximum concentration was less, with only about a 14 ppbv average compared to the 20 ppbv average of the full campaign. Unlike the data averaged over the full CalNex campaign that was used to derive the diurnal scaling factors, during this 7-day period the baseline CMAQ simulation described above was in reasonable agreement with the surface observations between 12:00 and 18:00 PDT (mean bias of 2.1 ppbv), but showed significant overestimates of NH_x (up to 50 ppbv) at all other times.

Despite applying the scaling factor to all emissions instead of solely to the feedlots as in Bash et al. (2013), the CMAQ predictions using the adjusted emission scenario shown as the red lines in Figure 8b (for $NH_{4(p)}$) and Figure 8c (for NH_x) match the measurements (black line) better than the original CARB inventory (blue line) over the day and night, consistent with Bash et al. (2013), with the mean night-time bias reduced by about a factor of 2. As the NH_x concentrations are dominated by $NH_{3(g)}$, $NH_{4(p)}$ has little impact on total NH_x results, as can be seen in the small amount of $NH_{4(p)}$ in Figure 8b (< 1 ppbv). Furthermore, model errors in $NH_{4(p)}$ reflect not only model errors in total NH_x, but also errors in the formation of HNO_3 and H_2SO_4 in the model. However, $NH_{4(p)}$ do not show similar improvement to NH_x when the improved diurnal cycle is used, with mixing ratios decreasing between the unadjusted and adjusted scenarios at night by 0.4 ppbv and remaining relatively unchanged during the day. The remaining night-time NH_x errors are significant, and may be due to the underestimate of vertical mixing at night in the model (see Section 4.2) or an underestimate of deposition (see Section 4.4) rather than a further overestimate of night-time emissions. Between 12:00 and 18:00 PDT there is a small increase in the model bias (1.2 ppbv) when the adjusted emissions are used, which is to be expected as we are increasing NH_3 emissions in this period. However, the changes are relatively small, and may reflect a slight overestimate of the total monthly NH_3 emissions in the CARB inventory during this period.

Two TES transects on 28 and 30 of May occurred during our case study time period. The changes in the model predicted NH_x values were small at the TES overpass time (less than 10 %), thus there was a correspondingly small change in the ratio of modelled RVMR and TES RVMR, changing from a factor of 2.4 to a factor of 2.1.

Atmos. Chem. Phys. Discuss., doi:10.5194/acp-2016-44, 2016
Manuscript under review for journal Atmos. Chem. Phys.
Published: 9 March 2016

Atmospheric Chemistry and Physics Discussions

4.4 Evaluation of bi-directional ammonia in CMAQ

Gas-phase NH_3 can either be deposited to or emitted from the surface depending on the land-type, land-use, and ambient concentrations (Bash et al., 2015; Fowler et al., 2009). The maximum and minimum points in NH_3 concentrations in the ground measurements (Figure 8c) correspond to the maximum and minimum wind speeds and temperatures measured. These highs and lows do not, however, line up in the model, suggesting there may be a need to better represent the vertical NH_3 fluxes, which can be done by utilizing the bi-directional NH_3 flux exchange scheme in CMAQ. Using the initial CARB emissions inventory we ran CMAQv5.0.2 with the inclusion of the calculation of the bi-directional NH_3 exchange to test the scheme's prediction of NH_3 concentrations in the SJV. We can see in Figures 8b and 8c that the run including bi-directional NH_3 flux (green line) increases NH_3 during the daytime, as expected due to the decrease in deposition during this time frame. At night, however, concentrations decreased compared to the initial run with the CARB emissions inventory due to an increase in modelled NH_3 deposition, leading to a reduction in net vertical flux of NH_3 at night. Bi-directional ammonia calculations also reduce the CMAQ RVMR to TES RVMR bias to a factor of 1.7 for the two over-passes during the case-study (from a factor of 2.4), consistent with Zhu et al. (2015a) who also looked at the impact of bidirectional exchange on RVMR in the SJV. These results are similar to the adjusted emissions case study discussed in Section 4.3, however the remaining over-estimate at night indicates a need for both a reduction in emissions at night and an inclusion of bi-directional ammonia calculations in the model, which is further investigated in the next section.

4.5 Evaluation of adjusted emissions and bi-directional ammonia in CMAQ

Based on results from both the adjusted emissions scenario and bi-directional ammonia calculations it was clear that combining techniques could result in better agreement with measurements. Thus, Figure 8c also contains a model simulation showing the results from a CMAQ run (purple line) where we adjusted emissions with a diurnal pattern as in section 4.3, and also ran CMAQ with the bi-directional NH_3 flux scheme as in section 4.4. This configuration produced lower mixing ratios at night when compared to ground measurements while maintaining reasonable mixing ratios during the day, but with slight overestimation of NH_x between 3:00pm and 10:00pm. This resulted in an overall MB decrease from 14.91 ppb in the initial CARB run, to 3.99 ppb in these final simulations, over the 7-day period (Table 2). At the time of the TES overpass, measurement and satellite RVMR comparisons also improve, with a bias reduction from -2.55 ppb in the initial run to -1.24 ppb for the two overpasses during the 7 day period, lower than the other two model simulation comparisons (Table 2).

5 Conclusions

We used NH_3 retrievals from the NASA Tropospheric Emission Spectrometer, as well as surface and aircraft observations of $NH_{3(g)}$ and submicron $NH_{4(p)}$ gathered during the CalNex campaign, to evaluate the ability of the CMAQ model run with the CARB emission inventory to simulate ambient $NH_{3(g)}$ and $NH_{4(p)}$ concentrations in the San Joaquin Valley. We find that CMAQ simulations of NH_3 driven with the CARB inventory are qualitatively and spatially consistent with TES satellite

Atmos. Chem. Phys. Discuss., doi:10.5194/acp-2016-44, 2016
Manuscript under review for journal Atmos. Chem. Phys.
Published: 9 March 2016

Atmospheric Chemistry and Physics Discussions

observations, with a correlation coefficient (r^2) of 0.54. However, the surface observations at Bakersfield indicate a diurnal cycle in the model bias with CMAQ overestimating NH_3 at night by at times more than 50 ppbv and underestimating it during the day by up to 10 ppbv. The surface, satellite, and aircraft observations all suggest that the afternoon NH_3 emissions in the CARB inventory are underestimated by at least a factor of two, while the night-time overestimate of NH_3 is likely due to a combination of overestimated night-time NH_3 emissions, underestimated night-time deposition, and insufficient vertical mixing in the WRF meteorological fields used to drive CMAQ thus indicating that the diurnally-constant NH_3 emissions used by CARB in the SJV likely misrepresent the diurnal emission cycle. We used the surface observations at Bakersfield to derive an empirical diurnal cycle of NH_3 emissions in the SJV in which nighttime and midday emissions differed by about a factor of 4.5. Adding this diurnal profile to the CMAQ simulations while keeping the daily NH_3 emissions constant at the CARB values significantly improved the model performance at night, but sizable errors (up to 20 ppbv) in nighttime NH_3 remained, possibly due to remaining errors in vertical mixing at night. The model performance is slightly degraded during the afternoon (12:00 to 18:00 PDT) when the diurnal cycle is adjusted, but this may reflect relatively small (~20 %) errors in the total monthly NH_3 emissions in the CARB inventory rather than remaining errors in the diurnal cycle. We then ran a simulation with the original CARB inventory but utilizing the bi-directional ammonia scheme in CMAQ. This resulted in similar results as adjusting the emissions, with decreased overestimates at night and a slight overestimate during the day. When running CMAQ with both adjusted diurnal emissions and the bi-directional NH_3 flux scheme, the over-estimate at night is almost negligible, with a slight over-estimate during the day remaining, providing the best agreement with measurements overall. Our results indicate that both a diurnally-varying emissions and a bi-directional NH_3 flux scheme should be applied when modelling $NH_{3(g)}$ and $NH_{4(p)}$ in this region, with more research needed to improve the modelling of vertical mixing and the residual layer at night.

Acknowledgements

The authors thank Leo Ramirez and Jeremy Avise at CARB for the emissions inventory data they provided, as well as Eli Mlawer, Thomas Nehrkorn and Elizabeth Steinhubel of AER and Jesse Bash, Jim Kelly, and Kirk Baker of EPA for their valuable comments and discussions on this work. This work was funded by the NOAA Climate Program Office Atmospheric Chemistry, Carbon Cycle, & Climate (AC4) program through Grants NA130AR4310060 and NA140AR4310129 to CRL, JDH, KCP, and MJA of AER and DKH, MDT, and SLC of CU Boulder. Development and evaluation of the TES NH_3 retrieval was funded through NASA grants to KCP of AER such as Grant NNH08CD52C. Infrastructure support for the Bakersfield ground site was provided through CARB contract 08-316 to Ron C Cohen and Allen H Goldstein at the University of California, Berkeley. The collection and analysis of CalNex surface observations of $NH_{3(g)}$ at Bakersfield were funded by a University of Toronto Centre for Global Change Science award to MM and a NSERC graduate scholarship to TCV of the University of Toronto. We also wish to thank the NOAA P3 aircraft flight crew and technicians. The conclusions of this paper are the authors' only, and do not reflect NOAA or CARB policy.

References

Alvarado, M. J., Cady-Pereira, K. E., Xiao, Y., Millet, D. B., and Payne, V. H.: Emission Ratios for Ammonia and Formic Acid and Observations of Peroxy Acetyl Nitrate (PAN) in Biomass Burning Smoke As Seen By the Tropospheric Emission Spectrometer (TES), Atmosphere, 2, 633–654, doi:10.3390/atmos2040633, 2011.

Alvarado, M. J., Payne, V. H., Cady-Pereira, K. E., Hegarty, J. D., Kulawik, S. S., Wecht, K. J., Worden, J. R., Pittman, J. V., and Wofsy, S. C.: Impacts of updated spectroscopy on thermal infrared retrievals of methane evaluated with HIPPO data, Atmos. Meas. Tech., 8, 965–985, doi:10.5194/amt-8-965-2015, 2015.

Bahreini, R., Ervens, B., Middlebrook, A. M., Warneke, C., de Gouw, J. A., DeCarlo, P. F., Jimenez, J. L., Brock, C. A., Neuman, J. A., Ryerson, T. B., Stark, H., Atlas, E., Brioude, J., Fried, A., Holloway, J. S., Peischl, J., Richter, D., Walega, J., Weibring, P., Wollney, A. G., and Fehsenfeld, F. C.: Organic aerosol formation in urban and industrial plumes near Houston and Dallas, Texas, J. Geophys. Res., 114, D00F16, doi:10.1029/2008JD011493, 2009.

Baker, K. R., Misenis, C., Obland, M. D., Ferrare, R. A., Scarino, A. J., and Kelly, J. T.: Evaluation of surface and upper air fine scale WRF meteorological modeling of the May and June 2010 CalNex period in California, Atmos. Environ., doi:10.1016/j.atmosenv.2013.08.006, 2013.

Bash, J. O., Cooter, E. J., Dennis, R. L., Walker, J. T., and Pleim, J. E.: Evaluation of a regional air-quality model with bidirectional NH_3 exchange coupled to an agroecosystem model, Biogeosciences, 10, 1635–1645, doi:10.5194/bg-10-1635-2013, 2013.

Bash, J., Henze, D. K., Jeong, G.-R., Zhu, L., Cady-Pereira, K. E., Shephard, M. W., Luo, M., and Pinder, R. W.: The impact of the diurnal temporal allocation of ammonia emissions on air-quality model estimates of ambient ammonia and inorganic aerosol concentrations, in preparation, 2015. 4827, 4830, 4831

Beer, R., Shephard, M. W., Kulawik, S. S., Clough, S. A., Eldering, A., Bowman, K. W., Sander, S. P., Fisher, B. M., Payne, V. H., Luo, M., Osterman, G. B., and Worden, J. R.: First satellite observations of lower tropospheric ammonia and methanol, Geophys. Res. Lett., 35, L09801, doi:10.1029/2008GL033642, 2008.

Beusen, A. H. W., Bouwman, A. F., Heuberger, P. S. C., Van Drecht, G., and Van der Hoek, K. W.: Bottom-up uncertainty estimates of global ammonia emissions from global agricultural production systems, Atmos. Environ., 42, 6067–6077, 2008.

Bricker, S., Longstaff, B., Dennison, W., Jones, A., Boicourt, K., Wicks, C., and Woerner. J.: Effects of Nutrient Enrichment In the Nation's Estuaries: A Decade of Change. NOAA Coastal Ocean Program Decision Analysis Series No. 26. National Centers for Coastal Ocean Science, Silver Spring, MD, 328 pp, 2007.

Bukovsky, M. S. and Karoly, D. J.: A brief evaluation of precipitation from the North American Regional Reanalysis, J. Hydrometeor., 8, 837–846, 2007.

Carfrae, J. A., Sheppard, L. J., Raven, J., Stein, W., Leith, I. D., Theobald, A., and Crossley, A.: Early effects of atmospheric ammonia deposition on Calluna vulgaris (L.) hull growing on an ombrotrophic peat bog, Water Air Soil Pollut. Focus, 4, 229–239, 2004.

Carmichael, G.R., Tang, Y., Kurata, G., Uno, I., Streets, D., Woo, J.-H., Huang, H., Yienger, J., Lefer, B., Shetter, R., Blake, D., Atlas, E., Fried, A., Apel, E., Eisele, F., Cantrell, C., Avery, M., Barrick, J., Sachse, G., Brune, W., Sandholm, S., Kondo, Y., Singh, H., Talbot, R., Bandy, A., Thorton, D., Clarke, A. and Heikes, B. (2003). Regional-scale chemical transport modeling in support of the analysis of observations obtained during the TRACE-P experiment. Journal of Geophysical Research 108: doi: 10.1029/2002JD003117. issn: 0148-0227.

Carter, W. P. L.: Development of the SAPRC-07 chemical mechanism, Atmos. Environ., 44, 5324–5335, 2010a.

Carter, W. P. L.: Development of a condensed SAPRC-07 chemical mechanism, Atmos. Environ., 44, 5336–5345, 2010b.

Chen, F. and Dudhia, J.: Coupling an advanced land-surface–hydrology model with the Penn State–NCAR MM5 modeling system. Part I: Model implementation and sensitivity, Mon. Wea. Rev., 129, 569–586, 2001.

Clarisse, L., Coheur, P.-F., Prata, F., Hadji-Lazaro, J., Hurtmans, D., and Clerbaux, C.: A unified approach to infrared aerosol remote sensing and type specification, Atmos. Chem. Phys., 13, 2195-2221, doi:10.5194/acp-13-2195-2013, 2013.

Clough, S. A., Shepard, M. W., Worden, J., Brown, P. D., Worden, H. M., Mingzhao, L., Rodgers, C. D., Rinsland, C.P., Goldman, A., Brown, L., Kulawik, S. S., Eldering, A., Lampel, M., Osterman, G., Beer, R., Bowman, K., Cady-Pereira, K. E., and Mlawer, E. J.: Forward Model and Jacobians for Tropospheric Emission Spectrometer Retrievals, IEEE Trans. Geosci. Remote Sens., 44, 1308–1323, 2006.

Draxler, R. R. and. Hess, G. D.: An overview of the HYSPLIT_4 modeling system for trajectories, dispersion, and deposition, Aust. Meteorol. Mag., 47, 295–308, 1998.

Ellis, R. A., Murphy, J. G, Pattey, E., van Haarlem, R., O'Brien, J. M., and Herndon, S. C.: Characterizing a Quantum Cascade Tunable Infrared Laser Differential Absorption Spectrometer (QC-TILDAS) for measurements of atmospheric ammonia, Atmos. Meas. Tech., 3, 397–406, 2010.

Ellis, R. A., Murphy, J. G., Markovic, M. Z., VandenBoer, T. C., Makar, P. A., Brook, J., and Mihele, C.: The influence of gas-particle partitioning and surface-atmosphere exchange on ammonia during BAQS-Met, Atmos. Chem. Phys., 11, 133–145, doi:10.5194/acp-11-133-2011, 2011.

Fowler, D., Pilegaard, K., Sutton, M., Ambus, P., Raivonen, M., Duyzer, J., Simpson, D., Fagerli, H., Fuzzi, S., Schjoerring, J., Granier, C., Neftel, A., Isaksen, I., Laj, P., Maione, M., Monks, P., Burkhardt, J., Daemmgen, U., Neirynck, J., Personne, E., Wichink-Kruit, R., Butterbach-Bahl, K., Flechard, C., Tuovinen, J., Coyle, M., Gerosa, G., Loubet, B., Altimir, N., Gruenhage, L., Ammann, C., Cieslik, S., Paoletti, E., Mikkelsen, T., Ro-Poulsen, H., Cellier, P., Cape, J., Horvath, L., Loreto, F., Niinemets, U., Palmer, P., Rinne, J., Misztal, P., Nemitz, E., Nilsson, D., Pryor, S., Gallagher, M., Vesala, T., Skiba, U., Brueggemann, N., Zechmeister-Boltenstern, S., Williams, J., O'Dowd, C., Facchini, M., de Leeuw, G., Flossman, A., Chaumerliac, N., and Erisman, J.: Atmospheric composition change: Ecosystems-Atmosphere interactions, Atmos. Environ., 43, 5193–5267, doi:10.1016/j.atmosenv.2009.07.068, 2009.

Galloway, J. N., Townsend, A. R., Erisman, J. W., Bekunda, M., Cai, Z., Freney, J. R., Martinelli, L. A., Seitzinger, S. P., and Sutton, M. A.: Transformation of the Nitrogen Cycle: Recent Trends, Questions, and Potential Solutions, Science, 320, 889– 892, 2008.

Gilliland, A. B., Dennis, R. L., Roselle, S. J., and Pierce, T. E.: Seasonal NH3 emission estimates for the eastern United States based on ammonium wet concentrations and an inverse modeling method, J. Geophys. Res., 108, D15, 4477, doi:10.1029/2002jd003063, 2003.

Gilliland, A. B., Wyat Appel, K., Pinder, R. W., and Dennis, R. L.: Seasonal NH3 emissions for the continental United States: Inverse model estimation and evaluation, Atmos. Environ., 40, 4986–4998, 2006.

Heald, C. L., Collett Jr., J. L., Lee, T., Benedict, K. B., Schwandner, F. M., Li, Y., Clarisse, L., Hurtmans, D. R., Van Damme, M., Clerbaux, C., Coheur, P.-F., Philip, S., Martin, R. V., and Pye, H. O. T.: Atmospheric ammonia and particulate inorganic nitrogen over the United States, Atmos. Chem. Phys., 12, 10295–10312, doi:10.5194/acp-12-10295-2012, 2012.

Hegarty, J., Henderson, J., Lewis, J., McGrath-Spangler, E., Scarino, A. J., Ferrare, R., P. DeCola, P., and Welton, E.: Evaluating High-Resolution WRF Simulations of PBL Depth Using Observations from DISCOVER-AQ 2011, Meteorology and Climate – Modeling for Air Quality, September 16-18, 2015, Sacramento, CA, 2015.

Hensen, A., Loubet, B., Mosquera, J., van den Bulk, W. C. M., Erisman, J. W., Dämmgen, U., Milford, C., Löpmeier, F. J., Cellier, P., Mikuška, P., and Sutton, M.A.: Estimation of NH_3 emissions from a naturally ventilated livestock farm using local-scale atmospheric dispersion modelling, *Biogeosciences,* 6, 2847–2860, 10.5194/bg-6-2847-2009, 2009.

Henze, D. K., Seinfeld, J. H., and Shindell, D. T.: Inverse modeling and mapping US air quality influences of inorganic PM2.5 precursor emissions using the adjoint of GEOS-Chem, Atmos. Chem. Phys., 9, 5877–5903, 2009.

Hong, S.-Y., Noh, Y., and Dudhia, J.: A new vertical diffusion package with an explicit treatment of entrainment processes, Mon. Wea. Rev., 134, 2318–2341, 2006.

Hristov, A. N., Hanigan, M., Cole, A., Todd, R., McAllister, T. A., Ndegwa, P. M., and Rotz, A.: Review: Ammonia emissions from dairy farms and beef feedlots, Can. J. Anim. Sci., 91(1), 1–35, doi:10.4141/CJAS10034, 2011.

Hutzell, W. T., Luecken, D. J., Appel, K. W., and Carter, W. P. L.: Interpreting predictions from the SAPRC07 mechanism based on regional and continental simulations, Atmos. Environ., 46, 417– 429, 2012.

Iacono, M. J., Delamere, J. S., Mlawer, E. J., Shephard, M. W., Clough, S. A., and Collins, W. D: Radiative forcing by long-lived greenhouse gases: Calculations with the AER radiative transfer models, J. Geophys. Res., 113, D13103, 2008.

Kelly, J. T., Baker, K. B., Nowak, J. B., Murphy, J. G., Markovic, M. Z., VandenBoer, T. C., Ellis, R. A., Neuman, J. A., Weber, R. J., Roberts, J. M., Veres, P. R., de Gouw, J. A., Beaver, M. R., Newman, S., and Misenis, C.: Fine-scale simulation of ammonium and nitrate over the South Coast Air Basin and San Joaquin Valley of California during CalNex-2010, J. Geophys. Res. Atmos., 119(6), 3600–3614. ISSN 2169-897X. 2014.

Langford, A. O., Fehsenfeld, F. C., Zachariassen, J., and Schimel, D. S.: Gaseous ammonia fluxes and background concentrations in terrestrial ecosystems of the United States, Global Biogeochem. Cy., 6, 459–483, 1992.

Lapina, K., Henze, D. K., Milford, J. B., Huang, M., Lin, M., Fiore, A. M., Carmichael, G., Pfister, G., and Bowman, K.: Assessment of source contributions to seasonal vegetative exposure to ozone in the U.S., J. Geophys. Res. Atmos., 119, 324–340, doi:10.1002/2013JD020905, 2014.

Lewis, J. R., E. J. Welton, A. M. Molod, and E. Joseph: Improved boundary layer depth retrievals from MPLNET, J. Geophys. Res. Atmos., 118, 9870–9879, doi:10.1002/jgrd.50570, 2013.

Lonsdale, C. R., Stevens, R. G., Brock, C. A., Makar, P. A., Knipping, E. M., and Pierce, J. R.: The effect of coal-fired power-plant SO_2 and NO_X control technologies on aerosol nucleation in the source plumes, Atmos. Chem. Phys., 12, 2012, doi:10.5194/acp-12-11519-2012.

Markovic, M. Z., VandenBoer, T. C., and Murphy, J. G.: Characterization and optimization of an online system for the simultaneous measurement of atmospheric water-soluble constituents in the gas and particle phases, J. Environ. Monit., 14, 1872–1884, 2012.

Martin, S. T., Hung, H.-M., Park, R. J., Jacob, D. J., Spurr, R. J. D., Chance, K. V., and Chin, M.: Effects of the physical state of tropospheric ammonium-sulfate-nitrate particles on global aerosol direct radiative forcing, Atmos. Chem. Phys., 4, 183–214, doi:10.5194/acp-4-183-2004, 2004.

Mesinger, F., DiMego, G., Kalnay, E., Mitchell, K., Shafran, P. C., Ebisuzaki, W., Jovic, D., Woollen, J., Rogers, E., and Berbery, E. H.: North American regional reanalysis, B. Am. Meteorol. Soc., 87, 343–360, 2006.

Mlawer, E. J., Taubman, S. J., Brown, P. D., Iacono, M. J., and Clough, S. A.: RRTM, a validated correlated-k model for the longwave, J. Geophys. Res., 102, 16663–16682, 1997.

Moss, R. H., Edmonds, J. A., Hibbard, K. A., Manning, M. R., Rose, S. K., van Vuuren, D. P., Carter, T. R., Emori, S., Kainuma, M., Kram, T., Meehl, G. A., Mitchell, J. F. B., Nakicenovic, N., Riahi, K., Smith, S. J., Stouffer, R. J., Thomson, A. M., Weyant, J. P., and Wilbanks, T. J.: The next generation of scenarios for climate change research and assessment, Nature, 463, 747–756, doi:10.1038/nature08823, 2010.

Nehrkorn, T., Henderson, J., Leidner, M., M. Mountain, J. Eluszkiewicz, K. McKain, and S. C. Wofsy: WRF simulations of the urban circulation in the Salt Lake City area for CO_2 modeling, J. Appl. Meteor. Clim., 52, 323–340, 2013.

Nemitz, E., Milford, C., and Sutton, M. A.: A two-layer canopy compensation point model for describing bi-directional biosphere-atmosphere exchange of ammonia, Q. J. Roy. Meteor. Soc., 127, 815–833, 2001.

Nowak, J. B., Neuman, J. A., Bahreini, R., Brock, C. A., Middlebrook, A. M., Wollny, A. G., Holloway, J. S., Peischl, J., Ryerson, T. B., and Fehsenfeld, F. C.: Airborne observations of ammonia and ammonium nitrate formation over Houston, Texas, J. Geophys. Res., 115, D22304, doi:10.1029/2010JD01495, 2010.

Nowak, J. B., Neuman, J. A., Bahreini, R., Middlebrook, A. M., Holloway, J. S., McKeen, S. A., Parrish, D. D., Ryerson, T. B., and Trainer, M.: Ammonia sources in the California South Coast Air Basin and their impact on ammonium nitrate formation, Geophys. Res. Lett., 39, L07804, doi:1029/2012GL051197, 2012.

Paulot, F. and Jacob, D. J.: Hidden Cost of U.S. Agricultural Exports: Particulate Matter from Ammonia Emissions, Environ. Sci. Technol., 48(2), 903–8, doi: 10.1021/es4034793, 2014.

Payne, V. H., Clough, S. A., Shephard, M. W., Nassar, R., and Logan, J. A.: Information-centered representation of retrievals with limited degrees of freedom for signal: Application to methane from the Tropospheric Emission Spectrometer, J. Geophys. Res., 114, D10307, doi:10.1029/2008JD010155, 2009.

Pinder, R. W., Walker, J. T., Bash, J. O., Cady-Pereira, K. E., Henze, D. K., Luo, M., Osterman, G. B., and Shephard, M. W.: Quantifying spatial and seasonal variability in atmospheric ammonia with in situ and space-based observations, Geophys. Res. Lett., 38, L04802, doi:10.1029/2010GL046146, 2011.

Pope, C. A., Burnett, R. T., Thurston, G. D., Thun, M. J., Calle, E. E., Krewski, D., and Godleski, J. J.: Cardiovascular Mortality and Year-round Exposure to Particulate Air Pollution: epidemiological evidence of general pathophysiological pathways of disease, Circulation, 109, 71–77, 2004.

RoTAP: Review of Transboundary Air Pollution: Acidification, Eutrophication, Ground Level Ozone and Heave Metals in the UK. Contract Report to the Department for Environment, Food and Rural Affairs. Centre for Ecology & Hydrology, 2012.

Rodgers, C. D. and Connor, B. J.: Intercomparison of remote sounding instruments, J. Geophys. Res., 108, doi:10.1029/2002JD002299, 2003.

Ryerson, T. B., Andrews, A. E., Angevine, W. M., Bates, T. S., Brock, C. A., Cairns, B., Cohen, R. C., Cooper, O. R., de Gouw, J. A., Fehsenfeld, F. C., Ferrare, R. A., Fischer, M. L., Flagan, R. C., Goldstein, A. H., Hair, J. W., Hardesty, R. M., Hostetler, C. A., Jimenez, J. L., Langford, A. O., McCauley, E., McKeen, S. A., Molina, L. T., Nenes, A., Oltmans, S. J., Parrish, D. D., Pederson, J. R., Pierce, R. B., Prather, K., Quinn, P. K., Seinfeld, J. H., Senff, C. J., Sorooshian, A., Stutz, J., Surratt, J. D., Trainer, M., Volkamer, R., Williams, E. J., and Wofsy, S. C: The 2010 California Research at the Nexus of Air Quality and Climate Change (CalNex) field study, J. Geophys. Res. Atmos., 118, 5830–5866, doi:10.1002/jgrd.50331, 2013.

Sawycky, M., Boulton, J. W., Trask, T., Van Heyst, B., and McClellan, C.: BC Agricultural Air Emissions Inventory. Rep. No. 1302423. Vancouver: RWDI, 2014, BC Ministry of Agriculture, 2014.

Scarino, A. J., Obland, M. D., Fast, J. D., Burton, S. P., Ferrare, R. A., Hostetler, C. A., Berg, L. K., Lefer, B. L., Haman, C. L., Rogers, R. R., Butler, C. F., Cook, A. L., and Harper, D. B.: Comparison of mixed layer heights from airborne high

spectral resolution lidar, ground-based measurements, and the WRF-Chem model during CalNex and CARES, Atmos. Chem. Phys., 14, 5547–5560, doi:10.5194/acp-14-5547-2014, 2014.

Schiferl, L. D., Heald, C. L., Nowak, J. B., Holloway, J. S., Neuman, J. A., Bahreini, R., Pollack, I. B., Ryerson, T. B., Wiedinmyer, C., and Murphy, J. G.: An investigation of ammonia and inorganic particulate matter in California during the CalNex campaign, J. Geophys. Res. Atmos., 119, 1883–1902, doi:10.1002/2013JD020765, 2014.

Schlesinger, W.H., 2009. On the fate of anthropogenic nitrogen. Proceedings of the National Academy of Sciences, U.S 106, 203e208.

Shephard, M. W., Cady-Pereira, K. E., Luo, M., Henze, D. K., Pinder, R. W., Walker, J. T., Rinsland, C. P., Bash, J. O., Zhu, L., Payne, V. H., and Clarisse, L.: TES ammonia retrieval 25 strategy and global observations of the spatial and seasonal variability of ammonia, Atmos. Chem. Phys., 11, 10743–10763, doi:10.5194/acp-11-10743-2011, 2011.

Shephard, M. W. and Cady-Pereira, K. E.: Cross-track Infrared Sounder (CrIS) satellite measurements of tropospheric ammonia, Atmos. Meas. Tech., 8, 1323–1336, 2015 www.atmos-meas-tech.net/8/1323/2015/ doi:10.5194/amt-8-1323-2015, 2015.

Simon, H., Allen, D. T., and Wittig, A. E.: Fine particulate matter emissions inventories: Comparisons of emissions estimates with observations from recent field programs, J. Air & Waste Manage. Assoc., 58, 320–343, 2008.

Skamarock, W. C. and Klemp, J. B.: A time-split nonhydrostatic atmospheric model for weather research and forecasting applications, J. Comp. Phys., 227, 3465–3485, 2008.

Skjøth, C. A., Geels, C., Berge, H., Gyldenkærne, S., Fagerli, H., Ellermann, T., Frohn, L. M., Christensen, J., Hansen, K. M., Hansen, K., and Hertel, O.: Spatial and temporal variations in ammonia emissions – a freely accessible model code for Europe, Atmos. Chem. Phys., 11, 5221-5236, doi:10.5194/acp-11-5221-2011, 2011.

Skjøth, C. A. and Geels, C.: The effect of climate and climate change on ammonia emissions in Europe, Atmos. Chem. Phys., 13, 117-128, doi:10.5194/acp-13-117-2013, 2013.

Sun, K., Cady-Pereira, K., Miller, D. J., Tao, L., Zondlo, M. A., Nowak, J. B., Neuman, J. A., Mikoviny, T., Müller, M., Wisthaler, A., Scarino, A. J., and Hostetler, C. A.: Validation of TES ammonia observations at the single pixel scale in the San Joaquin Valley during DISCOVER-AQ, J. Geophys. Res. Atmos., 120, 5140–5154. doi: 10.1002/2014JD022846., 2015.

Tucker, S. C., Brewer, Wm. A., Banta, R. M., Senff, C. J., Sandberg, S. P., Law, D. C., Weickmann, A., and Hardesty, R. M. :Doppler lidar estimation of mixing height using turbulence, shear, and aerosol profiles, J. Atmos. Ocean Tech., 26, 673–688, 2009.

US Environmental Protection Agency: Our Nation's Air – Status and Trends through 2008, Washington, DC, 2010.

Van Damme, M., Clarisse, L., Heald, C. L., Hurtmans, D., Ngadi, Y., Clerbaux, C., Dolman, A. J., Erisman, J. W., and Coheur, P. F.: Global distributions, time series and error characterization of atmospheric ammonia (NH3) from IASI satellite observations, Atmos. Chem. Phys., 14, 2905–2922, doi:10.5194/acp-14-2905-2014, 2014.

Walker, J. M., Seinfeld, J. H., Clarisse, L., Coheur, P.-F., Clerbaux, C., and Van Damme, M.: Simulation of nitrate, sulfate, and ammonium aerosols over the United States, Atmos. Chem. Phys. Discuss., 12, 19499–19527, doi:10.5194/acpd-12-19499- 2012, 2012.

Walker, J. T., Jones, M. R., Bash, J. O., Myles, L., Meyers, T., Schwede, D., Herrick, J., Nemitz, E., and Robarge, W.: Processes of ammonia air–surface exchange in a fertilized *Zea mays* canopy, Biogeosciences, 10, 981–998, doi:10.5194/bg-10-981-2013, 2013.

Wecht, K. J., Jacob, D. J., Wofsy, S. C., Kort, E. A., Worden, J. R., Kulawik, S. S., Henze, D. K., Kopacz, M., and Payne, V. H.: Validation of TES methane with HIPPO aircraft observations: implications for inverse modeling of methane sources, Atmos. Chem. Phys., 12, 1823–1832, doi:10.5194/acp-12-1823-2012, 2012.

Wichink Kruit, R. J., Schaap, M., Sauter, F. J., van Zanten, M. C., and van Pul, W. A. J.: Modeling the distribution of ammonia across Europe including bi-directional surface–atmosphere exchange, Biogeosciences, 9, 5261-5277, doi:10.5194/bg-9-5261-2012, 2012.

World Health Organization, Health Effects of Particulate Matter, Europe, available at: http://www.euro.who.int/__data/assets/pdf_file/0006/189051/, last accessed: January 2016.

Wu, S-Y., Hub, J.-L., Zhang, Y., and Aneja, V. P.: Modeling atmospheric transport and fate of ammonia in North Carolina—Part II: Effect of ammonia emissions on fine particulate matter formation, Atmos. Environ., 42, 3437–3451, 2008.

Zhang, L., Wright, P. L., and Asman, W. A. H.: Bi-directional air-surface exchange of atmospheric ammonia – A review of measurements and a development of a big-leaf model for applications in regional-scale air-quality models, J. Geophys. Res., 115, D20310, doi:10.1029/2009JD013589, 2010.

Zhu, L., Henze, D. K., Cady-Pereira, K. E., Shephard, M. W., Luo, M., Pinder, R. W., Bash, J. O., and Jeong, G. R.: Constraining U.S. ammonia emissions using TES remote sensing observations and the GEOS-Chem adjoint model, J. Geophys. Res. Atmos., 118, 3355–3368, doi:10.1002/jgrd.50166, 2013.

Zhu, L., Henze, D., Bash, J., Jeong, G.-R., Cady-Pereira, K., Shephard, M., Luo, M., Paulot, F., and Capps, S.: Global evaluation of ammonia bi-directional exchange, Atmos. Chem. Phys. Discuss., 15, 4823–4877, doi:10.5194/acpd-15-4823-2015, 2015a.

Zhu, L., D. K. Henze, J. O. Bash, K. E. Cady-Pereira, M. W. Shephard, M. Luo, and S. L. Capps: Sources and impacts of atmospheric NH3: Current understanding and frontiers for modeling, measurements, and remote sensing in North America, Current Pollution Reports, 1(2), 95–116, 2015b.

Atmos. Chem. Phys. Discuss., doi:10.5194/acp-2016-44, 2016
Manuscript under review for journal Atmos. Chem. Phys.
Published: 9 March 2016

Atmospheric Chemistry and Physics Discussions

		NH_x				$NH_{3(g)}$		$NH_{4(p)}$	
Date	**Time (PDT)**	**Slope**	**r^2**	**MB (ppbv)**	**MNB (%)**	**MB (ppbv)**	**MNB (%)**	**MB (ppbv)**	**MNB (%)**
20100507	10:00-17:00	0.15+/-0.01	0.29	-19.23	-22.52	-17.71	-21.11	-0.26	-13.08
20100524	16:00-22:00	0.20+/-0.01	0.31	-1.95	2.01	-1.74	18.24	-0.14	-58.70
	16:00-18:00	0.68+/-0.05	0.77	-0.20	10.79	-0.04	32.46	-0.08	-53.19
	18:00-22:00	0.18+/-0.01	0.29	-2.40	-0.213	-2.24	14.65	-0.144	-60.1
20100616	13:00-18:00	0.30+/-0.02	0.43	-5.92	-8.98	-4.9	-3.59	0.24	-45.32
20100618	13:00-18:00	0.18+/-0.02	0.10	-8.12	18.97	-7.85	28.9	-0.26	-75.2

Table 1. Summary statistics of the modelled to measured NH_x concentration comparisons following the SJV flights, with mean bias (MB) and mean normalized bias (MNB) of $NH_{3(g)}$ and $NH_{4(p)}$ included. See Figures 1 and 5.

	NH_x		$NH_{3(g)}$		$NH_{4(p)}$	
Measurement datatset compared to CMAQ output	**MB (ppbv)**	**MNB (%)**	**MB (ppbv)**	**MNB (%)**	**MB (ppbv)**	**MNB (%)**
Bakersfield site (CARB run)	14.91	260.12	15.01	278.19	-0.1	34.69
Bakersfield site (bidi-adjusted)	3.99	82.76	4.13	92.73	-0.14	10.87
TES (CARB run NH_3 RVMR)			-2.53	-39.14		
TES (bidi-adjusted NH_3 RVMR)			-1.24	-19.6		

Table 2. Summary statistics of the modelled to measured NH_x concentration comparisons to the ground measurements and TES RVMR with 1) the original CARB emissions inventory runs and 2) the bi-directional ammonia scheme runs with adjusted emissions for our 7-day case study period. Note as TES only observes $NH_{3(g)}$ there are no statistics for $NH_{4(p)}$ and NH_x from TES.

Atmos. Chem. Phys. Discuss., doi:10.5194/acp-2016-44, 2016
Manuscript under review for journal Atmos. Chem. Phys.
Published: 9 March 2016

Atmospheric Chemistry and Physics Discussions

a

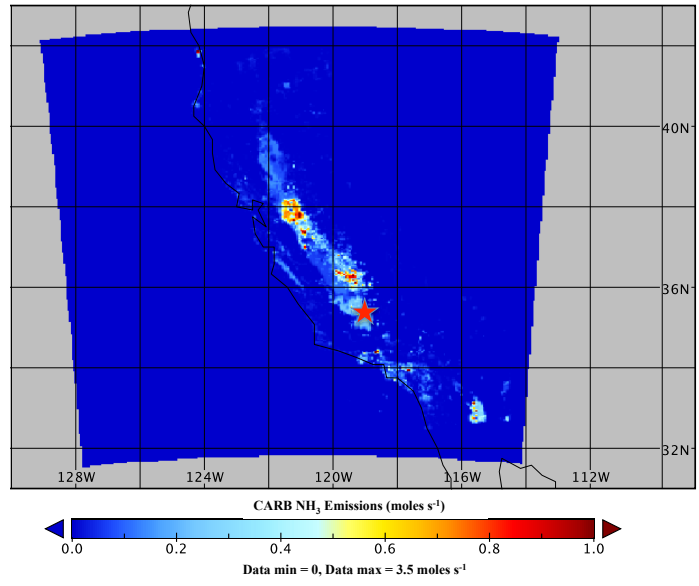

b)

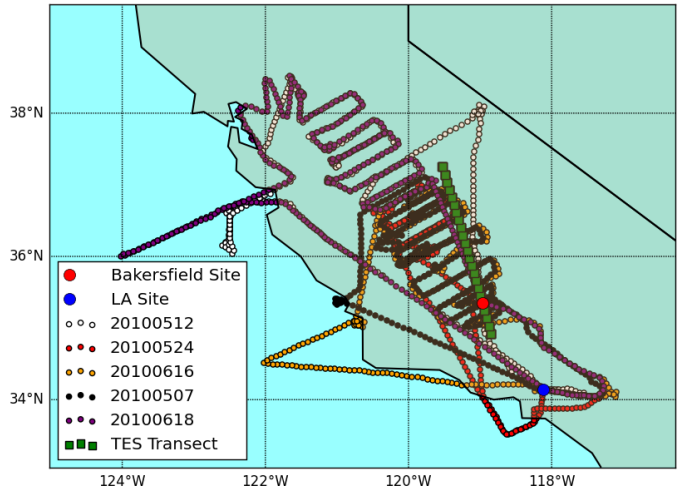

5 Figure 1a) Distribution of NH_3 emissions across the CMAQ domain for May 12, 2010 at 19:00 UTC. 1b) Selected P3 flight tracks (small circles), TES transect (green squares), Bakersfield site (red dot) and LA site (blue dot).

Atmos. Chem. Phys. Discuss., doi:10.5194/acp-2016-44, 2016
Manuscript under review for journal Atmos. Chem. Phys.
Published: 9 March 2016

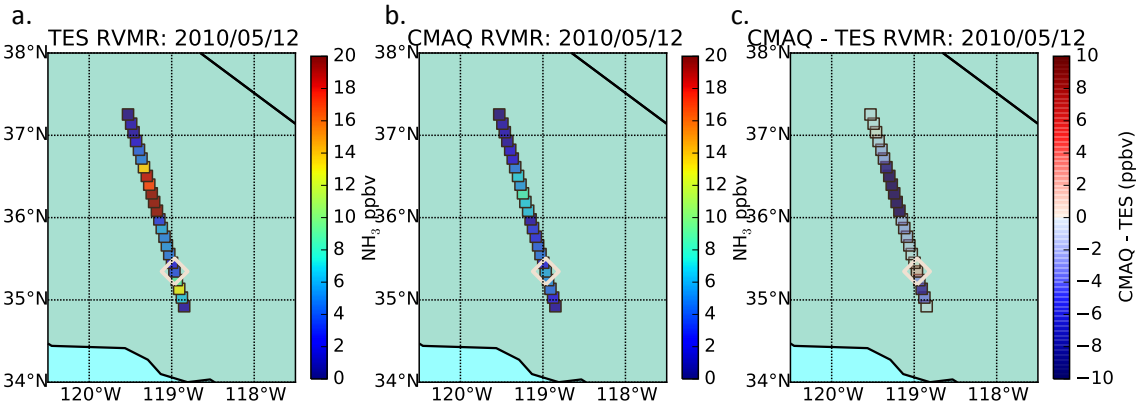

Figure 2. NH_3 representative volume mixing ratios (RVMRs) on 12 May 2010 during the CALNEX campaign for (a) TES special observations, (b) modelled RVMR for CMAQ and (c) the difference between each RVMR near the Bakersfield, CA, surface site with the white diamond locating the Bakersfield measurement site.

Atmos. Chem. Phys. Discuss., doi:10.5194/acp-2016-44, 2016
Manuscript under review for journal Atmos. Chem. Phys.
Published: 9 March 2016

Atmospheric Chemistry and Physics Discussions

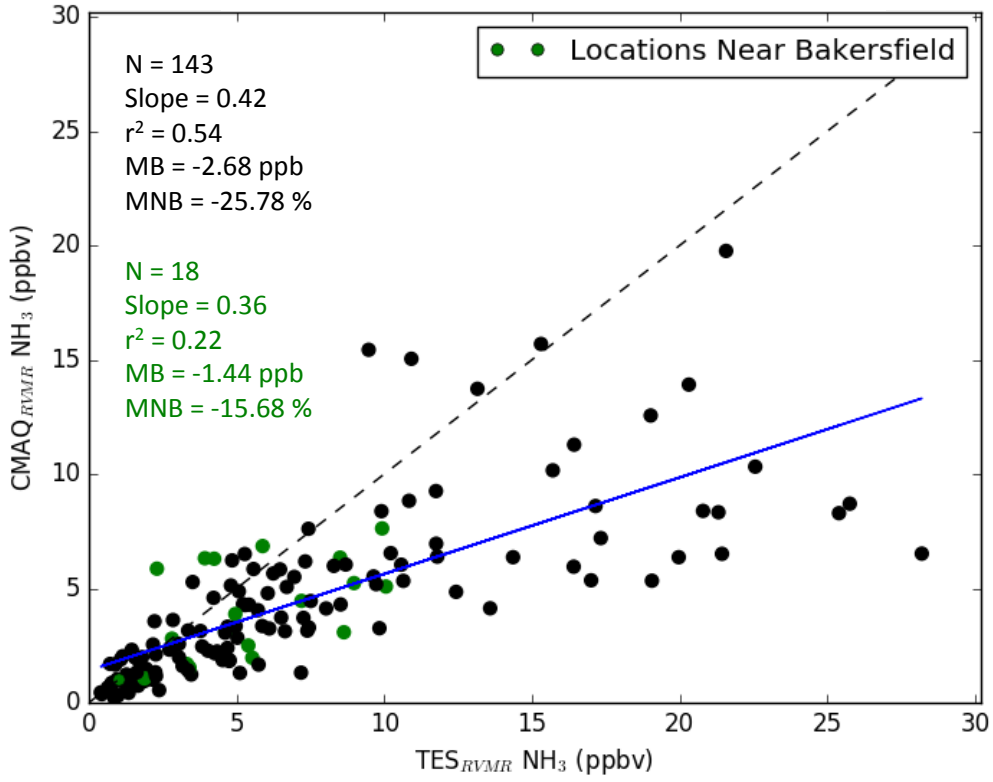

Figure 3. NH_3 representative volume mixing ratios for all TES special observation passes (TES_{RVMR}) during the CalNex campaign compared against modelled $CMAQ_{RVMR}$ (black dots). Green dots denote the overpasses closest to the Bakersfield measurement site. The statistics for the best-fit line, r^2, MB and MNB are in provided for each.

Atmos. Chem. Phys. Discuss., doi:10.5194/acp-2016-44, 2016
Manuscript under review for journal Atmos. Chem. Phys.
Published: 9 March 2016

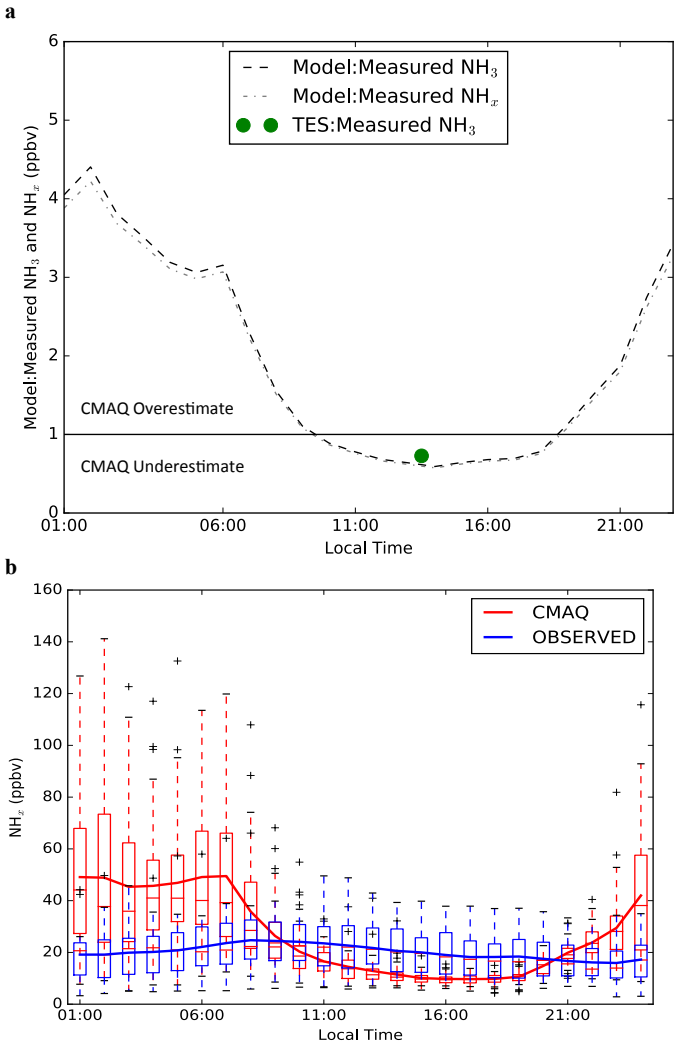

Figure 4. a) The average hourly ratio of modelled to measured NH_3 (dashed-dotted line) and NH_x (dashed line) mixing ratios at the Bakersfield ground site and the average modelled RVMR to TES RVMR ratio (green dot) in local PDT. b) Boxplot of average hourly modelled (red) and measured (blue) NH_x mixing ratios for the Bakersfield ground site, averaged over all measurement days during CalNex where the boxplots show the inter-quartile range and median line within the box and outliers (whiskers).

Atmos. Chem. Phys. Discuss., doi:10.5194/acp-2016-44, 2016
Manuscript under review for journal Atmos. Chem. Phys.
Published: 9 March 2016

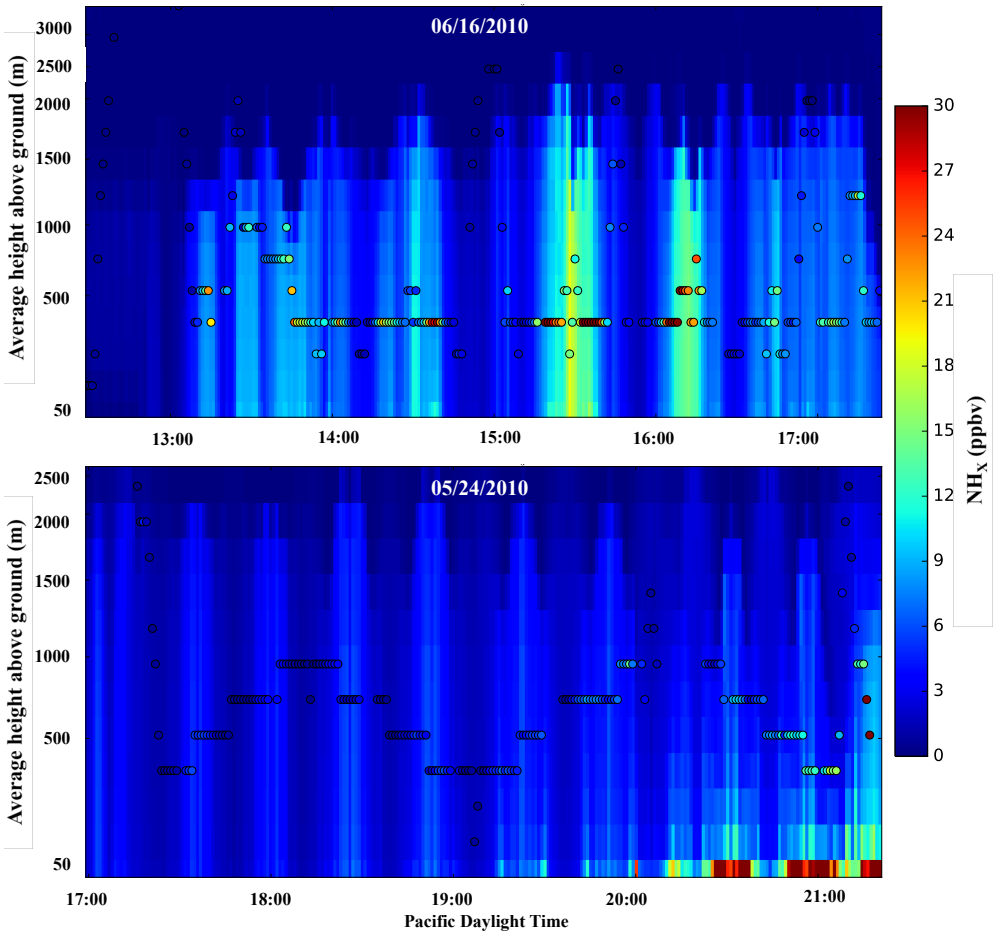

Figure 5. The hourly output of modelled NH_x is shown in the background with the measured 1 minute averaged NHx concentrations within the modelled hour shown as the dots. (a) The top plot is daytime flight over Bakersfield on June 16, 2010 between 10am and 6pm PDT and the (b) bottom plot is an evening flight on May 24, 2010 between 5pm and 9pm PDT.

5

Atmos. Chem. Phys. Discuss., doi:10.5194/acp-2016-44, 2016
Manuscript under review for journal Atmos. Chem. Phys.
Published: 9 March 2016

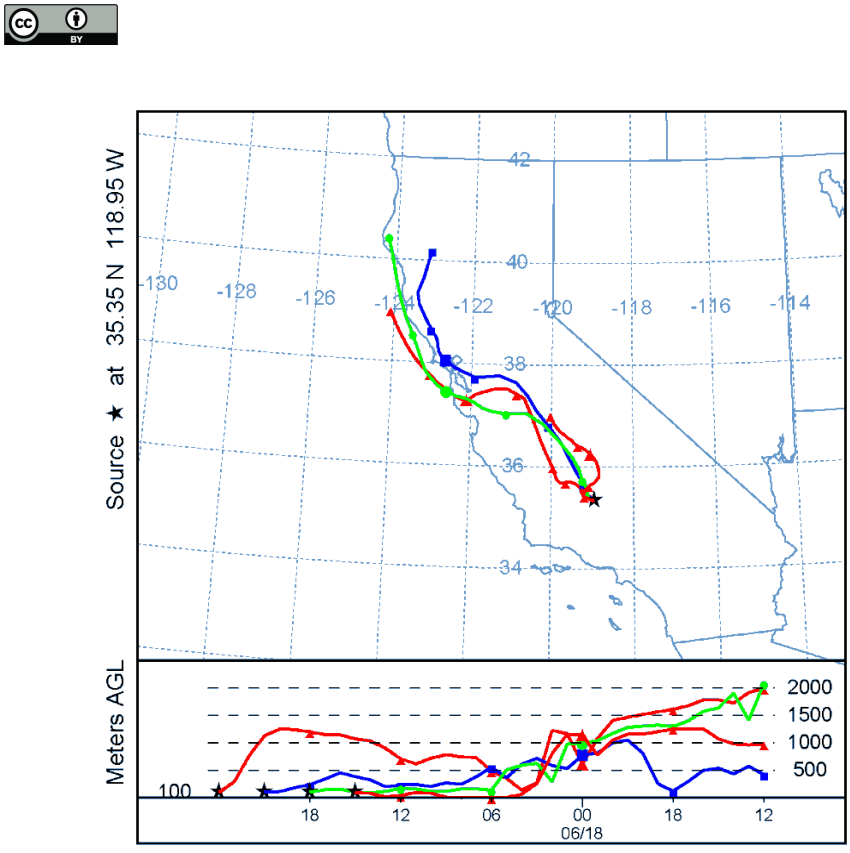

Figure 6. HYSPLIT back trajectories initiated from Bakersfield, CA generated using WRF 4 km input data. The back trajectories are initiated on June 18th at 17:00 PDT (red eastern-most in the top panel) and run backwards every 3 hours until June 17th at 20:00 PDT. Only the first 4 outputs are shown.

Atmos. Chem. Phys. Discuss., doi:10.5194/acp-2016-44, 2016
Manuscript under review for journal Atmos. Chem. Phys.
Published: 9 March 2016

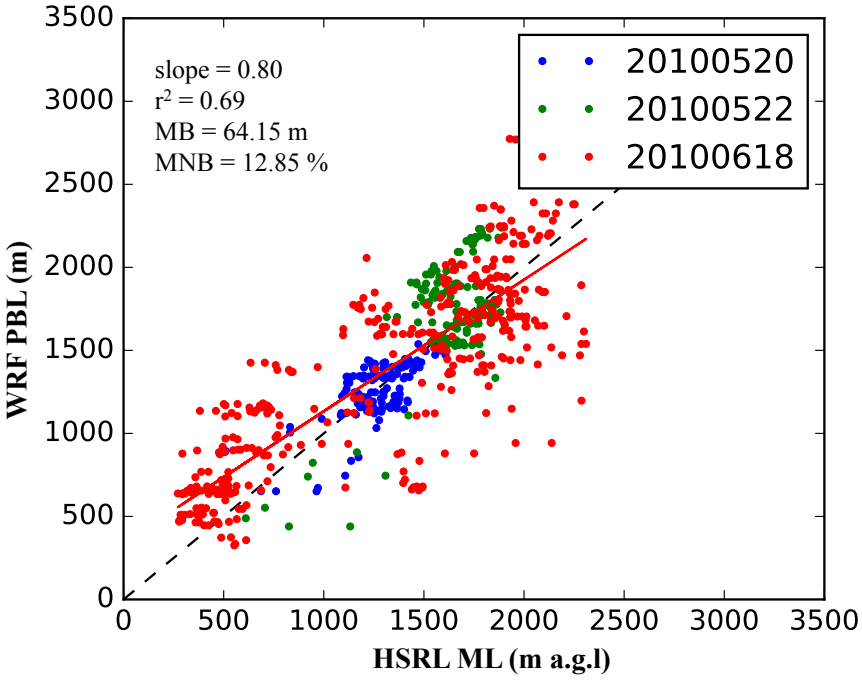

Figure 7. WRF predicted planetary boundary layer heights and HSRL calculated mixed layer heights for 3 flights in the San Joaquin Valley (2 during CalNex and one during a CARES campaign).

Atmos. Chem. Phys. Discuss., doi:10.5194/acp-2016-44, 2016
Manuscript under review for journal Atmos. Chem. Phys.
Published: 9 March 2016

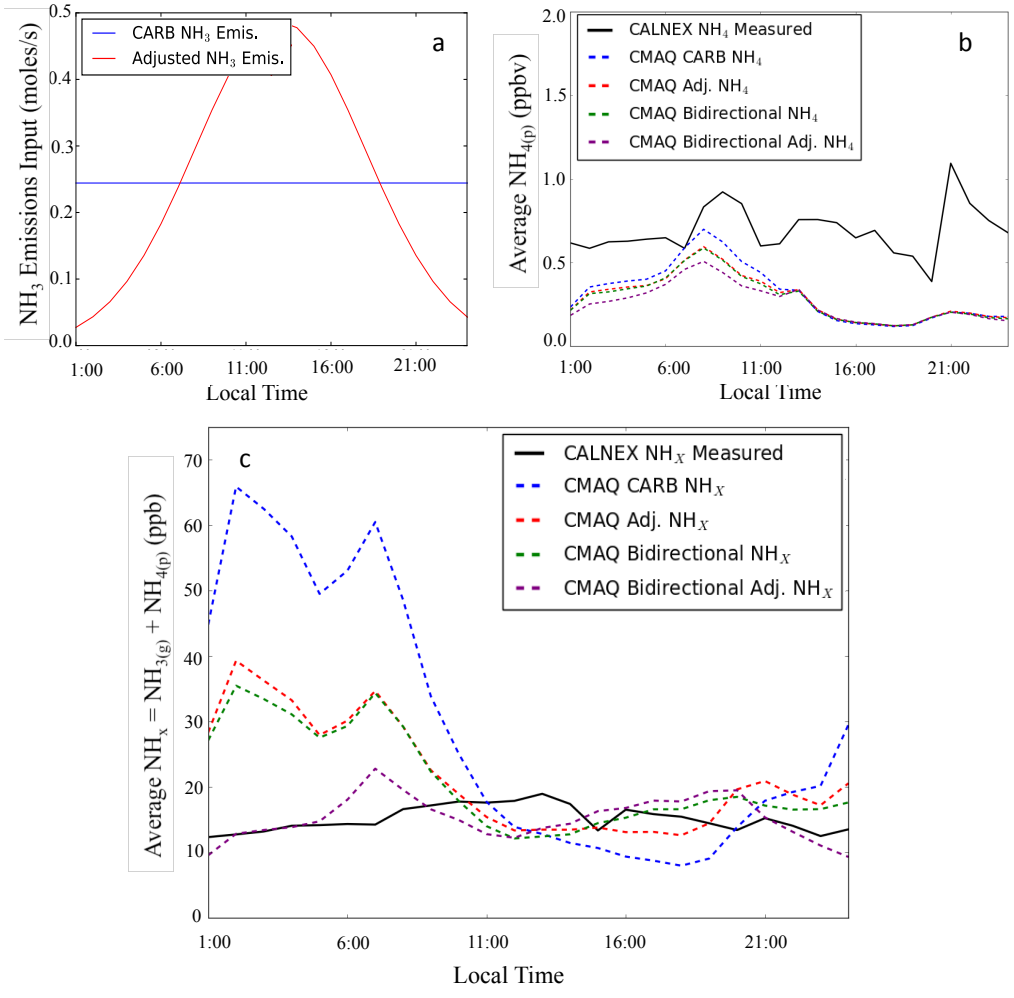

Figure 8. a) The CARB NH_3 emissions (solid blue) and adjusted scenario emissions (solid red) based on ground measurements at the Bakersfield site. b) Fine $NH_{4(p)}$ for the same time period to show the small concentrations relative to NH_3 (notice scale difference). c) NH_x concentrations for the CalNex measurements (solid black), the initial CMAQ run (dashed blue), an adjusted emissions CMAQ run (i.e., diurnally varying emissions, dashed red), a CMAQ run using the original emissions and the bi-directional NH3 flux scheme (dashed green), and a CMAQ run using both adjusted emissions and bi-directional flux (dashed purple) at the Bakersfield site averaged hourly from 25 to 31 of May, 2010.